Jurnal Penelitian Fisika dan Aplikasinya (JPFA) *Volume 11, Issue 01, June 2021*
p-ISSN: 2087-9946 DOI: 10.26740/jpfa.v?n?.p??-??
e-ISSN: 2477-1775 https://jpfa.unesa.ac.id

Research Article

Comparison of Bright Band Radar from GPM and MRR Observation in West Sumatera

Ravidho Ramadhan [1,a], Marzuki [1,b,*], Mutya Vonnisa[1,c], Harmadi [1,d], Hiroyuki Hashiguchi [2,e], and Toyoshi Shimomai [3,f]

[1] Department of Physics, Faculty of Mathematics and Natural Sciences, Universitas Andalas
Limau Manis, Pauh, Padang 25163, Indonesia
[2] Research Institute for Sustainable Humanosphere (RISH), Kyoto University
Yoshidahonmachi, Sakyo Ward, Kyoto 611-0011, Japan
[3] Remote Sensing Laboratory, Interdisciplinary Faculty of Science and Engineering, Shimane University
1060 Nishikawatsu-cho, Matsue-shi, Shimane 690-8504, Japan

e-mail: [a] ravidhoramadhan20@gmail.com, [b] marzuki@sci.unand.ac.id, [c] mutyavonnisa@sci.unand.ac.id,
[d] harmadi@sci.unand.ac.id, [e] hasiguti@rish.kyoto-u.ac.jp, and [f] shimomai@ecs.shimane-u.ac.jp
* Corresponding Author

Abstract

The Bright band (BB) observation can be used as an indication of the melting layer height. Measurement of BB from Normal Scan (NS) on Global Precipitation Measurement (GPM) had been compared with Micro Rain Radar (MRR), which is installed in Kototabang, West Sumatera (0.23° S; 100.32°E; 865 m above sea level). The GPM data were collected from December 2014 to June 2018 and compared with MRR observation from January 2012 to August 2016. The BB values from these instruments were compared with those recommended by the International Telecommunication Union Recommendation (ITU-R) P.839. The BB from GPM and MRR showed slightly diurnal and seasonal variations. BB observations from GPM and MRR show good agreement with slight diurnal and seasonal variations differences. BB observations are more similar when the intensity of solar radiation is lower, i.e., at night (18.00-24.00 LT) until early morning (00.00-06.00 LT). Furthermore, MRR showed a slight bimodal pattern in the seasonal variation, while GPM did not. Thus, the seasonal variation in the observation of both instruments is different. The most significant difference from the seasonal variation was observed in the summer season (June-August (JJA)). The mean BB of the two instruments is lower than the Freezing Height Level (FHL) value calculated from the ITU-R model. However, many BB from the two instruments (>36 %) have a BB altitude higher than FHL. Thus, the constant assumption of FHL in West Sumatera for the rain attenuation estimation of microwaves may not be appropriate.

Keywords: *Bright Band; GPM; MRR; Sumatera; diurnal variation; seasonal variation*

Perbandingan Bright Band dari Pengamatan GPM dan MRR di Sumatera Barat

Abstrak

Pengamatan Bright Band (BB) dapat mengindikasikan ketinggian melting layer. BB dari Global Precipitation Measurement (GPM) dengan Normal Scan (NS) scan telah dibandingkan dengan BB dari Micro Rain Radar (MRR) yang terpasang di Kototabang, Sumatera Barat ($0{,}23^0$ S; $10{,}32^0$ E; 865 m di

atas permukaan laut). Perbandingan BB dilakukan untuk data GPM dari Desember 2014 sampai Juni 2018 dan data MRR dari Januari 2012 sampai Agustus 2016. Hasil pengamatan BB dari kedua instrumen juga dibandingkan dengan nilai yang direkomendasikan oleh International Telecommunication Union Recommendation (ITU-R) P.839. Pengamatan BB dari GPM dan MRR di Sumatera Barat menunjukkan pola yang hampir sama dengan sedikit perbedaan pada variasi diurnal dan variasi musiman. Ketinggian BB dari GPM dan MRR menunjukkan nilai lebih seragam pada saat intensitas radiasi lebih sedikit yaitu pada malam hari (18.00-24.00 LT) hingga dini hari (00.00-06.00 LT). Kedua instrumen memperlihatkan pola variasi musiman yang berbeda. MRR menunjukkan pola bimodal untuk variasi musiman yang mana hal ini tidak teramati dari pengamatan GPM. Perbedaan nilai BB lebih kuat teramati pada musim panas yaitu selama Juli-Agustus (JJA). Pengamatan BB dari kedua instrumen mendapatkan banyak data Freezing Height Level (FHL) yang melebihi nilai yang diberikan ITU-R (>36 %). Hal ini menunjukkan penggunaan nilai FHL yang konstan sebagaimana direkomendasikan oleh model ITU-R menyebabkan estimasi atenuasi gelombang mikro di Sumatera Barat kurang akurat.

Kata Kunci: *Bright Band; GPM; MRR; variasi diurnal; variasi musiman*

PACS: 96.12.Jt; 84.40.Xb; 91.60.Qr; 78.70.Gq; 84.40.Ua.

Article History: Received: August 6, 2020 Aproved with minor revision: December 3, 2020
Accepted: July 18, 2021 Published: June 30, 2021

How to cite: Ramadhan R, et al. Comparison of Bright Band radar from GPM and MRR Observation in West Sumatera. *Jurnal Penelitian Fisika dan Aplikasinya (JPFA)*. 2021; **11**(1): 1-13. DOI: https://doi.org/10.26740/jpfa.

I. INTRODUCTION

Bright Band (BB) is a region of enhanced radar reflectivity in radar observation, indicating stratiform rain. The improved radar reflectivity is due to the increasing dielectric constant of drops from ice droplets into water droplets. Water in the ice phase has 0.19 dielectric constants, and water in the water phase has 0.9 dielectric constants. Therefore, radar reflectivity changes significantly. The BB arising area is also marked as a melting layer due to ice melting into raindrops. [1-2].

The illustration of BB can be seen in Figure 1. The top of BB height is the starting point of the melting process and indicates 0ºC isotherm level called Freezing High Level (FHL) [3]. Below the BB-Top, ice droplet melts into a large drop and then break into a smaller drop that returns the reflectivity radar to a decrease in the melting layer due to a strong dependence of reflectivity on the large-sized drop [4].

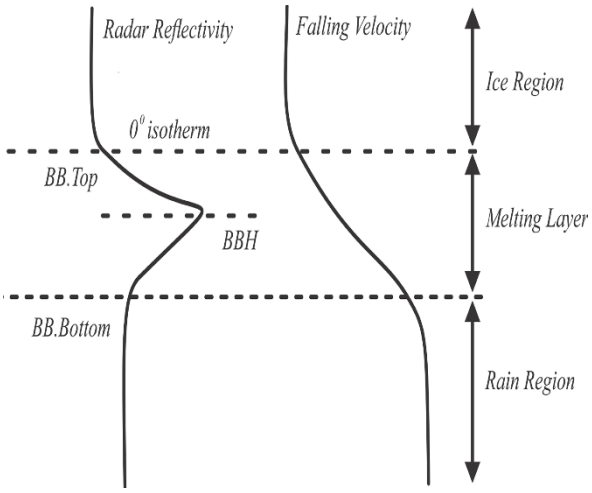

Figure 1. Typical of Bright Band Radar

The height of BB, which indicates the melting layer, is very important in microwave and millimeter telecommunication system design [5-7]. The melting layer's height is used to evaluate the signal attenuation in the rain region. An area's melting layer height usually refers to

the International Telecommunication Union Regulation (ITU-R) model. The ITU-R model assumes a constant melting layer height for one particular region and all rainfall intensities. The ITU-R gives the value of FHL for an area or the BB-Top of the radar observation. The BB can be observed by using surface radar and satellite-based radar. [8-10].

The precipitation radar (PR) onboard the Tropical Rainfall Measurement Mission (TRMM) satellite provides Bright Band Height (BBH) and FHL. Although the height of BBH is close to the FHL value, which is between 200-300 meters below FHL, in some cases, the BB-Top is much different from the FHL of the ITU-R model[11-13]. It can be found in tropical region like Indonesia [14-16], which has a slightly larger BBH than the FHL value determined by ITU-R. The TRMM was replaced by Global Precipitation Measurement (GPM) in 2014 to give more comprehensive information on precipitation parameters, including BB-Top, BBH, and BB-Bottom [17-21]. It can observe the melting layer characteristics in more detail, but GPM can't give real-time data for all regions because of satellite movement. This limitation can be fixed by surface radar, but surface radar does not directly provide the BB information. Thus, this research compared the BB from space-borne radar and surface radar in a tropical region with a strong atmospheric variation.

In this work, the BB from GPM was compared with that from the surface radar installed at Kototabang, West Sumatera, namely the Micro Rain Radar (MRR). The MRR was used to compare BB from GPM because this instrument is a vertically pointing radar [22-26]. The comparison of both instruments has never been conducted in Indonesia. This comparison considers monthly and diurnal variations, which are significantly observed in Sumatera [16, 27-30]. Therefore, this study analyzes the variation of BB over West Sumatera from MRR and GPM observation. This study can be an additional reference for BB observation in the tropics, especially in West Sumatera.

II. METHOD

This section provides the instrument and data used in this research. The data filtering technique was also explained. Because we investigated the BB height, only data on stratiform rain were included in this analysis.

Data and Instrument

The data used in this work are from MRR observation at Kototabang, West Sumatera, Indonesia (0.23°S; 100.32°E; 865 m above sea level (ASL)) and GPM observation. The GPM level-2 for Normal Scan (NS) data in range 0.73° S – 0.27° N and 99.32° E – 101.32° E were used. The data from NS scan has more robust BB structure than other scan mode.

MRR is a Vertical Pointing Radar (VPR) that provides Raindrops Size Distribution (RSD) and integrated rain parameter in vertical range bin resolution. MRR used frequency modulated continuous wave (FMCW) and Doppler principle to provide vertical falling velocity without a minimum distance of ambiguity. FMCW radars measure differences in instantaneous frequency between the received and transmitted signals. Detailed MRR specifications can be found in several references [31]. Besides the RSD observation, MRR is also powerful to observe BB height.

The GPM is a Dual-frequency Precipitation Radar (DPR) that combines Ku-band (13.6 GHz) and Ka-band (35.5 GHz) Precipitation Radar (PR). GPM DPR works in three classifications (CSF) modules to classify rain, namely, two single-frequency (SF) – that is Ku-only or Ka-only modules,

and one dual-frequency (DF) module [32-34]. SF modules in GPM DPR are similar to the TRMM algorithm that classifies rain type into three categories: stratiform, convective, and others. On the other hand, the DF CSF module combines Ku-band and Ka-band to make a new method called the dual-frequency ratio method (DFRm) for detailed BB data [35-36]. This study used GPM DPR level-2 data in the DF module, including BB-Top, BBH, BB-Bottom, and BB's thickness.

Table 1. Instrument Specification

Radar Parameter	MRR	GPM
Radar System	FCMWF	DPR
Operating Frequency	24.1 GHz	13.6 GHz and 35.5 GHz
Time Resolution	60 s	-
Vertical Resolution	150 m	125 m
Range bin	31	176

MRR has a 150 m spatial resolution with 31 range gates covering from the ground surface to 4650 m above ground level (AGL) or 5500 m above sea level with 60 s temporal resolution. It differs from GPM DPR Level-2 data resolution with 125 m vertical spatial resolution and 49 swathes in the NS. The instrument specification is given in Table 1. This study analyzes MRR data observation from January 2012 to August 2016 and compares it with GPM data from December 2014 to June 2018. Optical Rain Gauge (ORG) observation at the same site from 2012 to 2016 was also used to compare the rainfall rate from MRR observation.

Retrieval of BB Parameters

Dominant parameters for measuring BB from MRR are radar reflectivity factor (Z) and falling velocity (v). MRR estimate Z and v in the function of RSD can be seen in Equation (1).

$$Z = \int_{D_{\min}}^{D_{\max}} N(D) D^6 dD \quad (1)$$

$$v(D) = (9.65 - 10.3\exp(-0.6D))\,\delta v(h) \quad (2)$$

where $N(D)$ is RSD, D is the raindrop diameter (mm), and $\delta v(h)$ is a height dependent density correction for the fall velocity. We only analyze MRR data if the rainfall rate recorded by ORG more than 0.1 mm h^{-1} at at the same time.

Several methods can be used to retrieve the BB from the MRR data. We used the gradient of falling velocity (GFV) as the BB indicator, following the method proposed by Wang et al. [22]. The BB parameters from this method were expressed in Equation (3) – (6).

$$BB_{BOTTOM} = \max(GFV); \quad (3)$$

$$BB_{TOP} = \max(Z_{(n+1)} - Z_{(n)}); \quad (4)$$

$$BBH = \max(Z_{(n)}); \quad (5)$$

$$BB_{THICKNESS} = BB_{TOP} - BB_{BOTTOM}. \quad (6)$$

The height of BB-Bottom was calculated by taking a range bin that has maximum GFV because the ice crystals melt, so raindrop falling velocity increases to a maximum value in BB-Bottom. The range bin with maximum GFV must be lower than the range bin with a maximum of Z, indicated by BBH. Respectively, if the range bin of Z's maximum is lower than the range bin of maximum GFV, this event does not have BB. Furthermore, the range bin of BB-Top must be higher than the range bin of the maximum Z that provides from the

maximum gradient of Z above BB-Bottom. Thus, BB thickness could be inferred from calculating the difference of height of BB-Top and BB-Bottom. The flow chart of the method was illustrated in Figure 2.

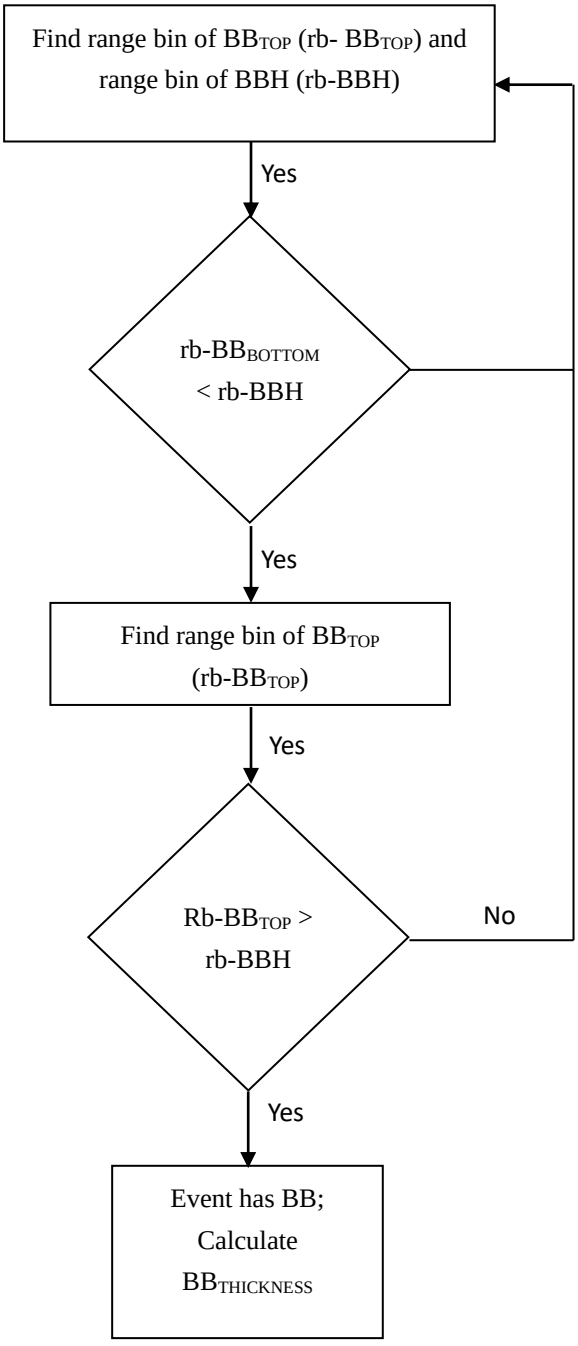

Figure 2. Flow Chart to Find BB from MRR Observation

The BB data from MRR was compared with BB data from GPM. The BB from GPM Level-2 data was downloaded from the National Aeronautics and Space Administration (NASA) official website (https://gpm.nasa.gov). We analyze the NS data with a 176 range bin. The data were filtered for a rainfall intensity of more than 0.1. We only analyze the data in 0.5 degrees from the MRR location. The GPM retrieves data into an ellipsoid, so the height of BB from MRR must be calibrated with the instrument's position above sea level. The mean of BB from MRR and GPM was compared on a diurnal and seasonal basis.

We also calculated the percentage error of BB between GPM and MRR observation using Equation (7).

$$\%error = \frac{|GPM - MRR|}{|MRR|} \times 100\% \quad (7)$$

We assumed the BB from MRR observation as reference value.

III. RESULTS AND DISCUSSION

The simultaneous observation of MRR and ORG was conducted over 8528 minutes, providing a substantial amount of stratiform rain data. As observed in our previous study [30], the variation of BB value with time basis is a crucial aspect of our findings. This variation in BB value, which measures the reflectivity of the rain, is attributed to the inherent instability of the atmosphere [37-38].

The average value of BB from MRR and GPM was given in Table 2. Generally, BB-Top from MRR is 4934 m above sea level (ASL) with a standard deviation of 151.66 m consistent with the ITU-R model P.836 for Indonesia. Its value is also consistent with some previous studies [9, 15-16] that calculated FHL using TRMM 2A25 data. However, it's worth noting that this value is slightly different from the previous study at Kototabang using MRR [39] that obtained FHL at 3.9 km above ground level (4.75 km ASL). This difference may be

attributed to the difference in method to classify the stratiform rain type, highlighting the potential impact of classification methods on the results.

Although the mean BB-Top from MRR observation is lower than the ITU-R model for the equator (5 km), More than 39 % of MRR data have FHL higher than 5 km. The highest and lowest BB-Top from MRR are 5350 m and 3950 m above sea level, respectively. Some variations in BB-Top, BBH, and BB-Bottom values from MRR observation were observed. The BBH from MRR varies from 3550 m to 5350 m above sea level. The difference between BB-Top and BBH (447 m) is close to previous studies [9-11]. The BB-Bottom from MRR varies from 3450 m to 3550 above sea level.

Table 2. Mean BB from GPM and MRR

	BB-Top (m ASL)	BBH (m ASL)	BB-Bottom (m ASL)
GPM (Standard Deviation)	4991 (287.77)	4531 (250.68)	4203 (266.89)
MRR (Standard Deviation)	4934 (151.66)	4487 (169.1)	4248 (170.5)
% error	1.16	0.98	1.06

The GPM obtained 3886 data for a 0.5-degree grid box around the MRR site. The distribution of GPM data was given in Figure 3. Generally, GPM estimates BB slightly higher than those obtained from MRR observation (Table 2). Although the value of BB-Top from GPM observation is higher than MRR observation, the average value is still lower than the FHL height of ITU-R model P.836 for Indonesia. Furthermore, the value of BBH from GPM observation is also higher than MRR observation. The range of BB-Top and BBH from GPM observation is similar to the MRR observation (460 m). Its value is consistent with previous studies [9-11]. Moreover, BB's value from both instruments shows a similar average value, which can be seen from a small percentage error of mean BB-Top, BBH, and BB-Bottom between GPM and MRR (Table 2).

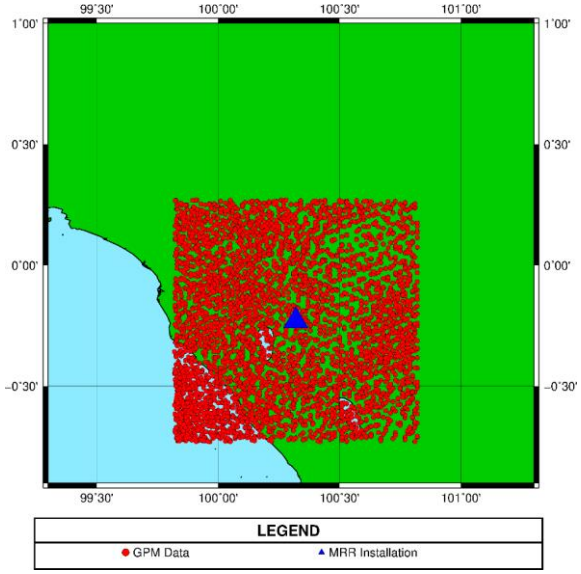

Figure 3. Data Distribution of GPM Data and MRR Location (Δ)

The values of BB from GPM vary significantly. The BB-Top of GPM varies from 2625 m to 6500 m. Moreover, BBH and BB-Bottom vary from 2238 to 6085 m for BBH and from 1875 m to 5750 m, respectively. This significant variation results in a large standard deviation of GPM observation. Thus, the BB data obtained by GPM of NS scan is more spreading compared to MRR. The GPM is likely less sensitive to light precipitation, which causes the miss identification of BB [17, 34, 36]. On the other hand, GPM obtained several BB data (74 data) with an altitude larger than MRR observation (5500 m above sea level). The BB in the tropics sometimes is higher [3, 16, 21, 23], but MRR can not detect it because of observation limitation. Therefore, GPM observation can inspect the higher BB than MRR. Besides, GPM also estimates a higher BB-Top than the ITU-R model with more than 36 % of data.

The strong variations in BB observation from both MRR and GPM observation are apparent. Some atmospheric variability may affect this variability. This research observed diurnal and seasonal variations in the as also found in some previous studies [27,29-30,40]. Thus, a constant BB assumption in the ITU-R model may be less accurate, especially at Kototabang, West Sumatera.

Diurnal Variation in BB

Diurnal variation is affected by a variation of solar radiation during day and night that involves the vertical variation of air temperature [40]. The variation of air temperature will be correlated to BB height variation [16, 41].

Figure 4a compares BB-Top and BB-Bottom at Kototabang, West Sumatera, from MRR and GPM observation on a diurnal basis. We exclude the hour with a small data number (< 5), such as at 05.00 and 10.00 Local Time (LT). The small data number does not provide confidence in average BB parameters.

The mean BB-Top from MRR is lower than FHL from the ITU-R model for the whole day, consistent with previous studies [15-16]. It is different from GPM with a strong variation mean of BB-Top. The average BB-Top shows that GPM estimates BB-Top slightly larger than MRR observation, particularly during 01.00 – 06.00 LT. During this period, the mean BB-Top exceeded the FHL determined by the ITU-R model in which the peak of BB Top is 5157 m (during 06.00 LT). Furthermore, the BB-Top from GPM decreases in the morning (06.00 – 12.00 LT), and the values are almost similar to MRR observation. During the daytime (12.00 – 18.00 LT), BB-Top from GPM is lower than MRR observation. The lowest BB-Top during daytime is 4668 m, which was observed at 14.00 LT. Moreover, the BB-Top and BB-Bottom show the most similar number during the night (06.00 – 12.00 LT). Although the hourly BB-Top and BB-Bottom are still different, GPM and MRR show a similar value, which a maximum percentage error of 3.08 for BB-Top and 3.27 for BB-Bottom.

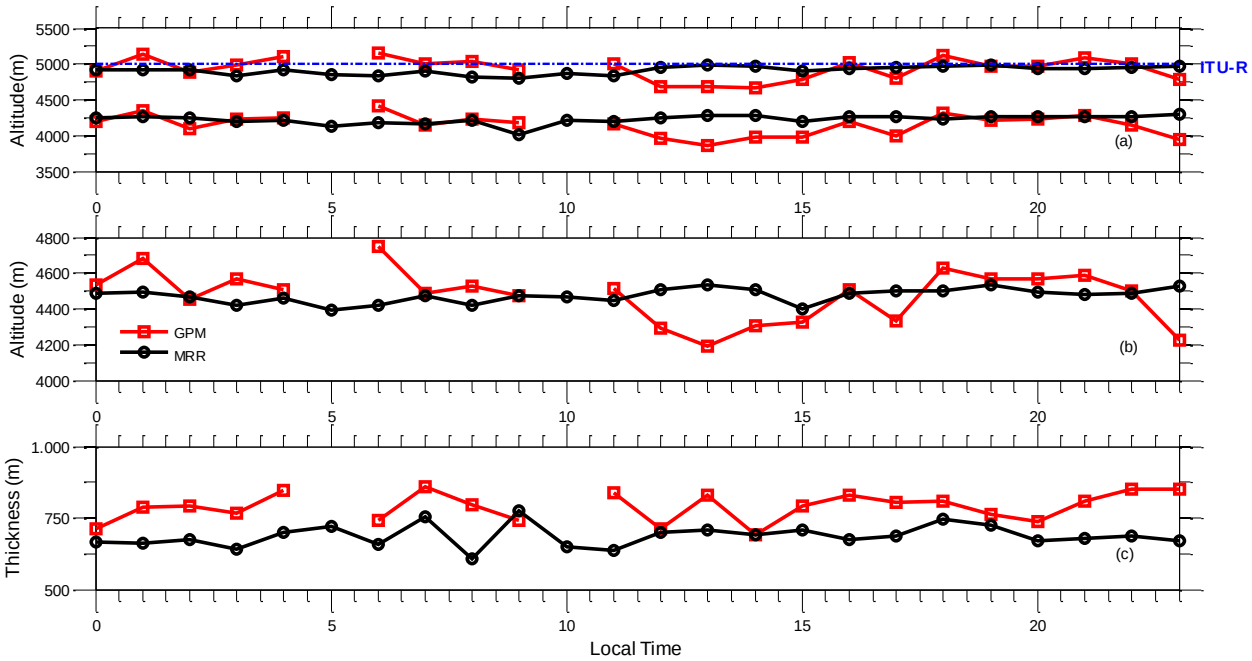

Figure 4. Diurnal Variation of BB from GPM and MRR Observations (a) BB-Top and BB-Bottom (b) BBH,

and (c) BB-Thickness

In addition to BB-Top and BB-Bottom, the BBH from GPM is also larger than that of MRR (Figure 4b). A significant difference is observed in BB-Thickness (Figure 4c). The BBH observation, in which the value from GPM is almost the same as that of MRR, is unique because GPM gives precisely the value for BBH while MRR gives the number of range bin location where BBH was observed. It is shown from the average percentage error of BBH from both instruments is only 3.54 % that is smaller than BB-Top and BB-Bottom. It is consistent with the lowest percentage error from the mean of BBH observation (Table 2). This feature means that the BBH algorithm is more accurate than BB-Top and BB-Bottom algorithm from GPM and MRR observation in diurnal variation.

The BB-Top and BB-Bottom measurement variation between GPM and MRR make BB-thickness from both instruments quite different. The GPM determined a larger BB-thickness than MRR observation (Figure 4c). The most considerable difference of BB-thickness of both GPM and MRR is 102 m. Thus, the two observations are in good agreement with each other in which the difference is lower than the range bin from MRR and GPM (Table 1) [43].

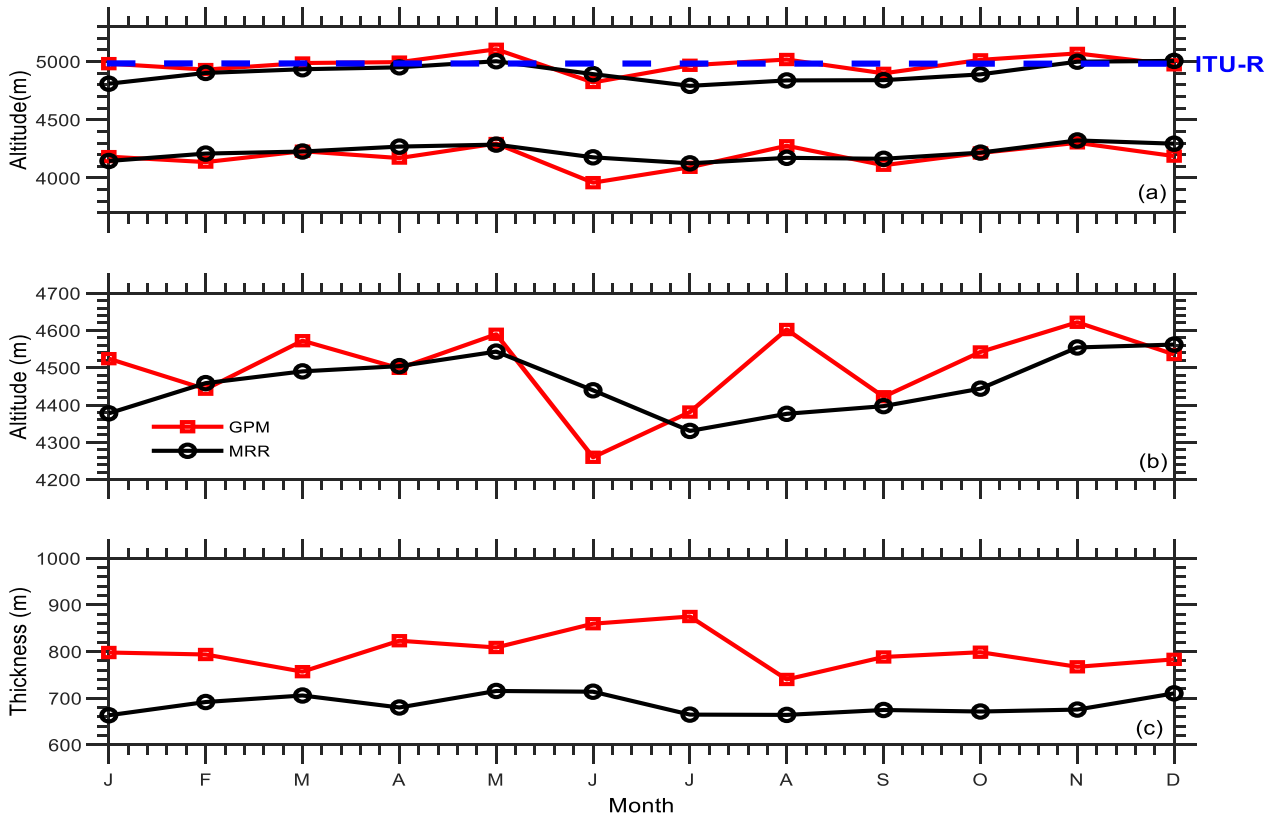

Figure 5. Seasonal Variation of BB from GPM and MRR Obsevation (a) BB-Top and BB-Bottom (b) BBH, and (c) BB-Thickness

Seasonal Variation in BB

To observe the seasonal variation of BB, the data were classified into winter on December – February (DJF), spring on March – Mei (MAM), summer on June – August (JJA), and Autumn on September – November (SON) [42]. Dwianda and Marzuki [15] found that FHL in Indonesia has a bimodal pattern that follows the sea surface temperature pattern. This feature slightly differs from GPM and MRR observations at Kototabang, West Sumatera, as shown in Figure 5. However, although it is not very significant, the bimodal pattern of seasonal variation in BB is slightly observed for MRR observation and less for GPM observation (Figure 5).

The GPM shows decreasing BB-Top and BB-Bottom values almost every season transition (DJF to MAM, MAM to JJA, and JJA to SON) and increasing values throughout the season. BB-Top height from GPM is 5 km in May, August, and November, with the highest peak in May (5104 m). Otherwise, a BB-Top peak was observed during DJF with a more than 5 km height in January (Figure 5a). Its peak decreased significantly in February (284 m), the most significant decreasing value during all months. It differs from MRR observation, which only gets an average BB-Top exceeding 5 km in May and December. The seasonal feature from MRR is quite similar to a previous study in Indonesia [15-16]. The difference in the seasonal pattern of GPM and MRR results in the difference in BB's value. The most different observation from both instruments for BB-Top and BB-Bottom was observed on JJA. Maximum percentage error was found in August for BB-Top (3.71 %) and in June for BB-Bottom (5.20 %). A more considerable difference in BB observation during summer is consistent with the diurnal variation in which more difference in BB observation was observed during higher solar radiation [16, 27-30].

BB-Thickness observation is more robust on the seasonal variation than diurnal variation.BB BB-Thickness observation is more robust on the seasonal variation than diurnal variation.

BB's variation was also identified from the monthly observation of BBH and BB-Thickness (Figure 5b and 5c). BBH from GPM and MRR is also most different during summer (JJA) and most similar during spring (MAM) like BB-Top and BB-Bottom. GPM determined larger BB-Thickness than MRR with a seasonal variation. The difference in BB-Thickness range from 51 m to 210 m with an average of 113.5 m. Thus, the difference of BB BB-Thickness observation is more robust on the seasonal variation than diurnal variation.

We have found the variability of BB observation from MRR and GPM level 2 with NS scanning. However, GPM has some other scan modes such as Match Scan (MS) and High-Sensitivity Scan (HS). This research is also limited to comparing BB observation from GPM and MRR from one location in Indonesia. Furthermore, the intra-seasonal variation of BB [44] is not included in the current analysis. Some of these limitations are being studied and will be published in other papers.

IV. CONCLUSION

The BB observations from GPM and MRR show good agreement with a slight difference in diurnal and seasonal variations (≤1.16 %). BB observations of the two instruments are similar when solar radiation intensity is lower, i.e., at night (18.00-24.00 LT) until the early morning (00.00-06.00 LT). The seasonal variation of BB observation of the two instruments is slightly different. The MRR observed a slight bimodal pattern in BB's seasonal variation, while GPM did not

show such a pattern. The most considerable difference in the seasonal variation was observed in the summer season (JJA). The GPM shows a larger thickness of BB than MRR observation due to the difference in both instruments' range bin. Moreover, the mean BB of the two instruments is lower than the Freezing Height Level (FHL) value calculated from the ITU-R model. However, many BB from the two instruments (>36 %) have a BB altitude higher than FHL. Thus, the constant assumption of FHL in West Sumatera for the rain attenuation estimation of microwaves may not be appropriate.

ACKNOWLEDGMENT

The present study was supported by 2020 Magister Thesis Research Grants from the Ministry of Research, Technology, and Higher Education (Contract no: T/ 11/ UN.16.17/ PT.01.03/ PTM-Kebencanaan/2020). The observation of MRR at Kototabang was supported by RISH Kyoto University. Furthermore, thanks to NASA for providing open-source GPM Level-2 data. Special thanks to Aldo Novaznursyah C, Velli Shinta and Novia Anggraini for their help in this work.

REFERENCES

[1] Fabry F and Zewadzki I. Long-Term Radar Observation of the Melting Layer of Precipitation an Their Interpretation. *Journal of the Atmospheric Science*. 1995; **52**(7): 838-851. DOI: https://doi.org/10.1175/1520-0469(1995)052%3C0838:LTROOT%3E2.0.CO;2.

[2] White AB, Gottas DJ, Stream ET, Ralph FM, and Neiman PJ. An Automated Bright Band Height Detection Algorithm for Use with Doppler Radar Spectral Moment. *Journal of Atmospheric Oceanic Technology*. 2002; **19**(5): 687-697. DOI: https://doi.org/10.1175/1520-0426(2002)019%3C0687:AABHDA%3E2.0.CO;2.

[3] Thurai M, Deguchi E, Iguchi T, and Okamoto KI. Freezing Height Distribution in the Tropics. *International Journal of Satellite Communications and Networking*. 2003; **21**(6): 533-545. DOI: https://doi.org/10.1002/sat.768.

[4] Uijlenhoet R and Pomeroy JH. Raindrop Size Distribution and Radar Reflectivity? Rain Rate Relationship for Radar Hydrology. *European Geoscience Union*. 2001; **5**(4): 615-628. DOI: https://doi.org/10.5194/hess-5-615-2001.

[5] Chakravarty K and Maitra A. Rain Attenuation Studies Over an Earth–Space Path at a Tropical Location. *Journal of Atmospheric and Solar-Terrestrial Physics*. 2010; **72**(1): 135-138. DOI: https://doi.org/10.1016/j.jastp.2009.10.018.

[6] Carlin JT and Ryzhkov AV. Estimation of Melting-Layer Cooling Rate from Dual-Polarization Radar: Spectral Bin Model Simulations. *Journal of Applied Meteorology and Climatology*. 2019; **58**(7): 1485-1508. DOI: https://doi.org/10.1175/JAMC-D-18-0343.1.

[7] Wolfensberger D, Scipion D, and Berne A. Detection and Characterization of the Melting Layer Based on Polarimetric Radar Scans. *Quarterly Journal of the Royal Meteorological Society*. 2016; **142**(1): 108-124. DOI: https://doi.org/10.1002/qj.2672.

[8] Cha JW, Chang KH, Yum SS, and Choi YJ. Comparison of the Bright Band Characteristics Measured by Micro Rain Radar (MRR) at a Mountain and a Coastal Site in South Korea. *Advances in Atmospheric Sciences*. 2009; **26**(2): 211-221. DOI: https://doi.org/10.1007/s00376-009-0211-0.

[9] Olurotimi EO, Sokoya O, Ojo JS, and Owolawi PA. Observation of Bright-Band Height Data from TRMM-PR for Satellite Communication in South Africa. *Journal of Atmospheric and Solar-Terrestrial Physics*.

2017; **160**: 24-33. DOI: https://doi.org/10.1016/j.jastp.2017.05.004.

[10] Carlin JT and Rhyzkov AV. Estimation of Melting-Layer Cooling Rate from Dual-Polarized Radar: Spectral Bin Model Simulations. *Journal of Applied Meteorology and Climatology*. 2019; **58**(7): 1485-1508. DOI: https://doi.org/10.1175/JAMC-D-18-0343.1.

[11] Awaka J, Iguchi T, and Okamoto K. TRMM PR Standard Algorithm 2A23 and its Performance on Bright Band Detection. *Journal of the Meteorological Society of Japan*. 2009; **87A**: 31-52. DOI: https://doi.org/10.2151/jmsj.87A.31.

[12] Yuan F, Lee YH, Meng YS, Manandhar S, and Ong JT. High-Resolution ITU-R Cloud Attenuation Model for Satellite Communications in Tropical Region. *IEEE Transactions on Antennas and Propagation*. 2019; **67**(9): 6115-6122. DOI: https://doi.org/10.1109/TAP.2019.2916746.

[13] Wang F, Liu H, Dong W, Zhang Y, and Meng Q. Characteristics of Lightning Flashes Associated with the Charge Layer Near the 0 C Isotherm in the Stratiform Region of Mesoscale Convective Systems. *Journal of Geophysical Research: Atmospheres*. 2018; **123**(17): 9524-9541. DOI: https://doi.org/10.1029/2018JD028569.

[14] Ramachandran V and Kumar V. Modified Rain Attenuation Model for Tropical Regions for Ku-Band Signals. *International Journal of Satellite Communication and Networking*. 2007; **25**(1): 53-67. DOI: https://doi.org/10.1002/sat.846.

[15] Dwianda R and Marzuki. Karakteristik melting layer di Indonesia berdasarkan radar hujan yang terpasang di satelit TRMM. *Jurnal Ilmu Fisika*. 2018; **10**: 73-82. DOI: https://doi.org/10.25077/jif.10.2.73-82.2018.

[16] Marzuki, Hashiguchi H, and Vonnisa M, Harmadi, and Muzirwan. Long-Term Change in Rainfall Rate and Melting Layer Height in Indonesia. *Progress in Electromagnetics Research Symposium*. 2018; 1154-1158. DOI: https://doi.org/10.23919/PIERS.2018.8597606.

[17] Awaka J, Le M, Chandrasekar V, Yoshida N, Higashiuwatoko T, Kubota T, and Iguchi T. Rain Type Classification Algorithm Module For GPM Dual-Frequency Precipitation Radar. *Journal of Atmospheric and Oceanic Technology*. 2016; **33**(9): 1887-1898. DOI: https://doi.org/10.1175/JTECH-D-16-0016.1.

[18] Gong J and Wu D. Microphysical Properties of Frozen Particles Inferred from Global Precipitation Measurement (GPM) Microwave Imager (GMI) Polarimetric Measurements. *Atmospheric Physics and Chemistry*. 2017; **17**(4): 2741-2757. DOI: https://doi.org/10.5194/acp-17-2741-2017.

[19] Casella D, Panegrossi G, Sanò P, Marra AC, Dietrich S, Johnson BT, and Kulie MS. Evaluation of the GPM-DPR Snowfall Detection Capability: Comparison with CloudSat-CPR. *Atmospheric Research*. 2017; **197**: 64-75. DOI: https://doi.org/10.1016/j.atmosres.2017.06.018.

[20] Kotsuki S, Terasaki K, and Miyoshi T. GPM/DPR Precipitation Compared with a 3.5-km-Resolution NICAM Simulation. *Sola*. 2014; **10**: 204-209. DOI: https://doi.org/10.2151/sola.2014-043.

[21] Kobayashi K, Shige S, and Yamamoto MK. Vertical Gradient of Stratiform Radar Reflectivity Below the Bright Band from the Tropics to the Extratropical Latitudes Seen by GPM. *Quarterly Journal of the Royal Meteorological Society*. 2018; **144**(S1): 165-175. DOI: https://doi.org/10.1002/qj.3271.

[22] Rico-Ramirez MA and Cluckie ID. Bright-Band Detection from Radar Vertical Reflectivity Profiles. *International Journal of Remote Sensing*. 2007; **28**(18): 4013-4025. DOI:

https://doi.org/10.1080/01431160601047797.

[23] Sumesh RK, Resmi EA, Unnikrishnan CK, Jash D, Sreekanth TS, Resmi MM, Rajeevan K, Nita S, and Ramachandran KK. Microphysical Aspects of Tropical Rainfall during Bright Band Events at Mid and High-Altitude Regions over Southern Western Ghats, India. *Atmospheric Research*. 2019; **227**: 178-197. DOI: https://doi.org/10.1016/j.atmosres.2019.05.002.

[24] Jash D, Resmi EA, Unnikrishnan CK, Sumesh RK, Sreekanth TS, Sukumar N, and Ramachandran KK. Variation in Rain Drop Size Distribution and Rain Integral Parameters during Southwest Monsoon Over a Tropical Station: An Inter-Comparison of Disdrometer and Micro Rain Radar. *Atmospheric Research*. 2019; **217**: 24-36. DOI: https://doi.org/10.1016/j.atmosres.2018.10.014.

[25] Marzuki, Hashiguchi H, Shimomai T, Rahayu I, and Vonnisa M. Performance Evaluation of Micro Rain Radar Over Sumatra through Comparison with Disdrometer and Wind Profiler. *Progress In Electromagnetics Research*. 2016; **50**: 33-46. DOI: https://doi.org/10.2528/PIERM16072808.

[26] Wang H, Lei H, and Yang J. Microphysical Processes of a Stratiform Precipitation Event Over Eastern China: Analysis Using Micro Rain Radar Data. *Advances in Atmospheric Sciences*. 2017; **34**(12): 1472-1482. DOI: https://doi.org/10.1007/s00376-017-7005-6.

[27] Marzuki, Kozu T, Shimomai T, Randeu WL, Hashiguchi H, and Shibagaki Y. Diurnal Variation of Rain Attenuation Obtained from Measurement of Raindrop Size Distribution in Equatorial Indonesia. *IEEE Transactions on Antennas and Propagation*. 2009; **57**(4): 1191-1196. DOI: https://doi.org/10.1109/TAP.2009.2015812.

[28] Marzuki, Nauval F, and Hashiguchi H. Regional and Diurnal Variation of Rain Attenuation Obtained from Measurement of Raindrop Size Distribution Over Indonesia at Ku, Ka and W bands. *Progress in Electromagnetics Research*. 2017; **57**: 25-34. DOI: https://doi.org/10.2528/PIERM17030503.

[29] Ramadhan R, Marzuki, Vonnisa M, Harmadi, Hashiguchi H, and Shimomai T. Seasonal Variation in the Vertical Profile of the Raindrop Size Distribution for Stratiform Rain as Inferred From Micro Rain Radar Observation at Kototabang. *AIP Conference Proceeding*. 2020; **2221**(1): 090002. DOI: https://doi.org/10.1063/5.0003181.

[30] Ramadhan R, Marzuki, Vonnisa M, Harmadi, Hashiguchi H, and Shimomai T. Diurnal Variation in the Vertical Profile of the Raindrop Size Distribution for Stratiform Rain as Inferred from Micro Rain Radar Observations in Sumatra. *Advances in Atmospheric Sciences*. 2020; **37**(8), 832-846. DOI: https://doi.org/10.1007/s00376-020-9176-9.

[31] Peters G, Fischer B, and Andersson T. Rain Observation with a Vertically Looking Micro Rain Radar (MRR). *Boreal Environment Research*. 2002; **7**(4): 353-362. Available from: http://sensovant.com/productos/pdf/meteorologia/pluviometria-hielo/sensovant-lluvia-observaciones-con-radar.pdf.

[32] Gao J, Tang G, and Hong Y. Similarities and Improvements of GPM Dual-Frequency Precipitation Radar (DPR) upon TRMM Precipitation Radar (PR) in Global Precipitation Rate Estimation, Type Classification and Vertical Profiling. *Remote Sensing*. 2017; **9**(11): 1142. DOI: https://doi.org/10.3390/rs9111142.

[33] Suzuki K, Kamamoto R, Nakagawa K, Nonaka M, Shinoda T, Ohigashi T, Minami Y, Kubo M, and Kaneko Y. Ground Validation of GPM DPR Precipitation Type

Classification Algorithm by Precipitation Particle Measurements in Winter. *SOLA*. 2019; **15**: 94-98. DOI: https://doi.org/10.2151/sola.2019-018.

[34] Seto S and Iguchi T. Intercomparison of Attenuation Correction Methods for the GPM Dual-Frequency Precipitation Radar. *Journal Atmospheric and Oceanic Technology*. 2015; **32**(5): 915-926. DOI: https://doi.org/10.1175/JTECH-D-14-00065.1.

[35] Le M and Chandrasekar V. Hydrometeor Profile Characterization Method for Dual-Frequency Precipitation Radar on Board the GPM. *IEEE Transactions on Geoscience Remote Sensing*. 2013a; **51**(6): 3648-3658. DOI: https://doi.org/10.1109/TGRS.2012.2224352.

[36] Le M and Chandrasekar V. Precipitation Type Classification Method for Dual-Frequency Radar (DPR) Precipitation Radar on Board the GPM. *IEEE Transactions on Geoscience Remote Sensing*. 2013b; **51**(3): 1784-1790. DOI: https://doi.org/10.1109/TGRS.2012.2205698.

[37] Williams E and Renno N. An Analysis of the Conditional Instability of the Tropical Atmosphere. *Monthly Weather Review*. 1993; **121**(1): 21-36. DOI: https://doi.org/10.1175/1520-0493(1993)121%3C0021:AAOTCI%3E2.0.CO;2.

[38] Mishin VV and Tomozov VM. Kelvin–Helmholtz Instability in the Solar Atmosphere, Solar Wind and Geomagnetosphere. *Solar Physics*. 2016; **291**(11): 3165-3184. DOI: https://doi.org/10.1007/s11207-016-0891-4.

[39] Ramadhan R and Marzuki M. Distribusi Arah Vertikal Butiran Hujan dari Hujan Stratiform di Kototabang dari Pengamatan Micro Rain Radar (MRR). *Jurnal Fisika Unand*. 2019; **8**(3): 252-259. DOI: https://doi.org/10.25077/jfu.8.3.252-259.2019.

[40] Kozu T, Reddy K K, Mori S, Thurai M, Ong J T, Rao D N, and Shimomai T. Seasonal and Diurnal Variations of Raindrop Size Distribution in Asian Monsoon Region. *Journal of the Meteorological Society of Japan. Ser. II*. 2006; **84A**: 195-209. DOI: https://doi.org/10.2151/jmsj.84A.195.

[41] Chakraborty R, Basha G, and Ratnam MV. Diurnal and Long-Term Variation of Instability Indices Over a Tropical Region in India. *Atmospheric Research*. 2018; **207**: 145-154. DOI: https://doi.org/10.1016/j.atmosres.2018.03.012.

[42] Tangang F, Salimun E, Aldrian E, Sopaheluwakan A, and Juneng L. ENSO Modulation of Seasonal Rainfall and Extremes in Indonesia. *Climate Dynamics*. 2018; **51** (7-8): 2559-2580. DOI: https://doi.org/10.1007/s00382-017-4028-8.

[43] Gao J, Tang G, and Hong Y. Similarities and Improvements of GPM Dual-Frequency Precipitation Radar (DPR) upon TRMM Precipitation Radar (PR) in Global Precipitation Rate Estimation, Type Classification and Vertical Profiling. *Remote Sens*. 2017; **9**(11): 1142. DOI: https://doi.org/10.3390/rs9111142.

[44] Marzuki, Hashiguchi H, Vonnisa, M. Harmadi, and Katsumata M. Determination of Intraseasonal Variation of Precipitation Microphysics in the Southern Indian Ocean from Joss–Waldvogel Disdrometer Observation during the CINDY Field Campaign. *Advance in Atmospheric Sciences*. 2018; **35**: 1415–1427. DOI: https://doi.org/10.1007/s00376-018-8026-5.